

Optically dim counterparts of hard X-ray selected AGNs[★]

R. Maiolino¹, M. Salvati¹, L.A. Antonelli², A. Comastri³, F. Fiore², F. Ghinassi⁴, R. Gilli⁵,
F. La Franca⁶, F. Mannucci⁷, G. Risaliti⁵, D. Thompson⁸, and C. Vignali^{3,9}

¹ Osservatorio Astrofisico di Arcetri, Largo E. Fermi 5, I-50125 Firenze, Italy

² Osservatorio Astronomico di Roma, via Frascati 33, I-00040, Monteporzio Catone (Roma), Italy

³ Osservatorio Astronomico di Bologna, via Ranzani 1, I-40127, Bologna, Italy

⁴ Telescopio Nazionale Galileo, Aptdo de Correos 565, E-38700 Santa Cruz de La Palma, Canary Islands, Spain

⁵ Dipartimento di Astronomia e Scienza dello Spazio, Università di Firenze, Largo E. Fermi 5, I-50125 Firenze, Italy

⁶ Dipartimento di Fisica, Università “Roma Tre”, via della Vasca Navale 84, I-00146 Roma, Italy

⁷ CAISMI-CNR, Largo E. Fermi 5, I-50125 Firenze, Italy

⁸ California Institute of Technology, MS 320-47, Pasadena, CA, 91125, USA

⁹ Dipartimento di Astronomia, Università di Bologna, via Ranzani 1, I-40127, Bologna, Italy

Received / Accepted

Abstract. We present near-IR photometry and imaging observations of a small sample of sources identified in the BeppoSAX 5–10 keV survey (HELLAS) which resolves $\sim 20 - 30\%$ of the X-ray background at these energies. The near-IR data are combined with optical spectra and photometry. Only 40% of the sources in our sample have the blue, power law continuum typical of color-selected QSOs. The remaining 60% are dominated by a galactic component which, on the basis of the continuum colors and shape, have ages ranging from 10^9 to 10^{10} years. The images show that the blue QSOs are pointlike at our angular resolution, while all the other sources are extended, consistent with their spectral appearance and low redshift. Since down to $R = 20$ only about two thirds of the HELLAS sources have a counterpart, the preliminary HELLAS census comprises in roughly equal parts: i) blue QSOs (mostly at high redshifts); ii) optically dim, galaxy-dominated active nuclei (mostly at modest redshifts); and iii) empty fields (possibly highly absorbed QSOs at high redshifts).

Key words: X–rays: galaxies – Infrared: galaxies – Galaxies: active – diffuse radiation

1. Introduction

X-ray background (XRB) synthesis models ascribe most of the high energy flux to radio quiet, absorbed Active

Send offprint requests to: R. Maiolino

[★] Based on observations made with the Italian Telescopio Nazionale Galileo (TNG) operated on the island of La Palma by the Centro Galileo Galilei of the CNAA (Consorzio Nazionale per l’Astronomia e l’Astrofisica) at the Spanish Observatorio del Roque de los Muchachos of the Instituto de Astrofisica de Canarias.

Galactic Nuclei (AGNs) at intermediate and high redshifts (e.g. Comastri et al. 1995, Gilli et al. 1999, Pompilio et al. 2000). Observationally the available information on AGNs at these redshifts refers mostly to unabsorbed nuclei, since the current samples of radio quiet AGNs have been selected mostly with color techniques, or in the soft X rays. Only recently have selection criteria less sensitive to absorption been used. Examples are the radio quiet red QSOs (Kim & Elvis 1999), analogous to the ones already found in radio loud samples (eg. Webster et al. 1995), and the spectroscopic identifications in the ELAIS field (Rowan-Robinson et al. 1999). Yet, most of our knowledge about absorbed, radio quiet AGNs is limited to low redshifts and low luminosities, where spectroscopic surveys of bright galaxies have been performed.

The High Energy LLarge Area Survey [HELLAS, Comastri et al. 2000, Fiore et al. 2000 (paper II)] aims at providing a useful sample of hard X-ray selected (5–10 keV), optically identified AGNs while waiting for the Chandra and XMM results. The survey instrument is the BeppoSAX MECS. The sky coverage is 1–50 square degrees at $F_{5-10\text{ keV}} = 5-30 \times 10^{-14}\text{erg cm}^{-2}\text{s}^{-1}$, respectively, and is 84 deg^2 at fluxes higher than $9 \times 10^{-13}\text{erg cm}^{-2}\text{s}^{-1}$. The catalogued sources amount to 147, and at the fainter limit the source density is $16.9 \pm 6.4\text{ deg}^{-2}$, implying that about 20–30% of the XRB at these energies has been resolved. A program of optical identification is underway, which includes optical/near-IR broad band photometry and near-IR imaging, beside optical spectroscopy of all candidates down to $R = 20$. So far, 63 optical counterparts have been identified, in about two thirds of the examined errorboxes. About half of the spectra are typical of QSOs, with a blue continuum and broad lines, about half are of intermediate type (1.8–1.9), generally with red continua, and a few of them contain only narrow lines [Fiore et al. 1999 (paper I), La Franca et al. 2000 (paper III)].

Table 1. Observing log.

#	SAXJ	Date	Seeing (")	Sensit.(T_{int}) ^a	
				J	Ks
1	1118.8+4026A	19/02/99	1.0	21.2(4.0)	19.1(4.0)
2	2044.6-1028	22/07/99	0.4	21.8(1.6)	21.0(1.6)
3	1117.8+4018	19/02/99	0.9	21.3(4.0)	18.9(2.0)
4	1118.8+4026B	19/02/99	1.0	21.2(4.0)	19.1(4.0)
5	0045.7-2515	18/12/98	1.6	20.9(6.3)	19.0(8.5)
6	1528.8+1939	02/03/99	1.0	—	19.3(5.8)
7	1519.5+6535	02/03/99	0.8	—	19.4(4.0)
8	1353.9+1820	19/02/99	1.0	20.8(2.0)	18.9(3.0)
9	1218.9+2958	19/02/99	0.9	20.9(2.0)	18.9(2.0)
10	1118.2+4028	19/02/99	1.0	20.8(2.0)	18.8(2.0)

^a 3σ limiting magnitude (within an aperture twice the seeing) and integration time in minutes.

In this paper we present and discuss preliminary results of the near-IR photometry and imaging observations of the spectroscopically identified counterparts. Combined with the optical information presented in papers I and III these data give a broad-band view of the properties of the HELLAS sources and allow a preliminary census of the hard XRB contributors.

2. The observations

Most of the near-IR images were obtained with the AR-NICA camera (Lisi et al. 1996) at the Italian National Telescope Galileo (TNG). Only one (#2) out of a total of 10 objects was observed with NIRC (Matthews & Soifer 1994) at Keck I. We observed these 10 objects at K-short ($\sim 2.16\mu\text{m}$) and 8 of them at J ($\sim 1.25\mu\text{m}$). Tab. 1 gives the observation log along with the limiting magnitudes reached in the exposures. The items are sorted according to the B-R color, which is a measure of the AGN dominance, as will be discussed in the following. The first column gives an identification number that, for sake of clarity, will be used in place of the full SAX name reported in column 2. Objects #1 and #4 are actually two QSOs that have been identified within the same errorbox of one of the HELLAS sources (paper I).

The observations were performed by mosaicing the field every minute, with offsets of 10-20" around the source, both to sample the background and to minimize the effects of artifacts in the array. The data reduction pipeline was similar to that described in Hunt et al. (1994). Each image was divided by a differential flat field made out of sky twilight images. Images of each mosaic were aligned by means of field stars and, then, coadded with a sigma clipping rejection to exclude hot and dead temporary pixels, not accounted for by the bad pixel mask.

In this paper we also take advantage of the optical spectra used to identify the sources (papers I and III). In particular we will use the information on the continuum shape and the equivalent width of the broad lines. Opti-

cal photometry of these objects was taken from various sources: Palomar sky survey, UKST sky survey and some new observations obtained at various telescopes in connection with the spectroscopic program. Each of these optical data set was obtained with slightly different filters, however we homogenized the data to the Johnson system by normalizing the observed spectra to the observed photometric points and then resampling in the Johnson bands.

3. Results and discussion

Tab. 2 gives the main results of our near-IR observations. Columns 2 to 4 give the X-ray properties, while columns 5 and 6 give properties inferred from the optical spectra and, in particular, spectral classification and redshift. Our subsample of HELLAS sources was not selected with a specific criterion, it consists of all the early HELLAS identifications known and accessible at the time of the observations. This subsample includes intermediate type (1.9) AGNs, "classical" broad line QSOs with blue continuum, "red" broad line QSOs, characterized by a red underlying continuum, and one LINER, i.e. all the HELLAS identified types. Our sample also covers the whole range of redshift of the parent sample. Thus, even if it is not statistically solid because of the small size, it still contains information on the general properties of the HELLAS sources. Column 10 gives the full-width at half-maximum of the near-IR image measured along the major axis. The source is labelled as resolved/extended in column 9 if it is at least two times wider than the seeing.

Narrow line AGNs, intermediate type AGNs and red QSOs all show extended emission indicative of a significant (near-IR) contribution of the host galaxy. Furthermore, the B-K colors are not clustered around the value of ~ 2 , typical of color-selected QSOs at high redshift, but extend to very red values up to B-K ~ 6 , in analogy with the radio selected AGNs (Webster et al. 1995). Therefore, our red AGNs can be considered the radio quiet counterpart of those found in the radio surveys. Instead, all and only blue QSOs are unresolved; as we shall see, this is a consequence of the dominance of the AGN component and, possibly, of their higher redshift. These findings are summarized in Fig. 1, where we plot R-K versus B-R and where point-like and extended sources are marked with circles and squares respectively. The solid oblique line is the locus of a single powerlaw, and the big cross marks the point where a powerlaw would give B-K = 2.1. The dotted line is the reddening curve for a QSO spectrum¹ at $z = 0.26$ (the average of the three reddest objects, #8, #9, and #10), starting from $AV=0.5$ for sake of clarity. The star gives the colors of an old stellar population², again

¹ We used the standard Galactic extinction curve and a QSO template derived from a combination of the average spectra given in Elvis et al. (1994) and Francis et al. (1991).

² The galaxy templates were taken from Bruzual & Charlot (1993), with solar abundances and a Salpeter IMF.

Table 2. Results.

#	F_X^a	$\log N_H^b$	L_X^c	type ^d	z	J^e	Ks^e	ext. ^f	FWHM ^g	B-R	B-Ks	R-Ks
1	1.2	< 22.5	45.1	B	1.13	17.98 ± 0.10	16.69 ± 0.15	N	$1''.3(1.3)$	0.42 ± 0.28	1.69 ± 0.29	1.27 ± 0.29
2	2.0	> 22.7	46.6	B	2.76	16.25 ± 0.05	14.91 ± 0.05	N	$0''.4(1.0)$	0.43 ± 0.28	2.88 ± 0.25	2.45 ± 0.25
3	1.3	$22.7^{+0.5}_{-0.5}$	45.4	B	1.27	19.38 ± 0.10	17.74 ± 0.15	N	$1''.0(1.1)$	0.55 ± 0.28	2.96 ± 0.29	2.41 ± 0.29
4	— ^h	< 22.4	— ^h	B	0.89	19.21 ± 0.10	17.44 ± 0.15	N	$1''.4(1.4)$	0.75 ± 0.28	3.23 ± 0.29	2.48 ± 0.29
5	3.5	$22.6^{+0.5}_{-0.5}$	43.3	1.9	0.11	16.38 ± 0.05	15.27 ± 0.07	Y	$5''.1(3.2)$	0.80 ± 0.28	2.83 ± 0.25	2.03 ± 0.25
6	1.4	< 22.6	43.3	L	0.18	—	15.94 ± 0.07	Y	$8''.9(8.9)$	1.22 ± 0.28	4.30 ± 0.25	3.08 ± 0.25
7	11.	$23.2^{+0.1}_{-0.1}$	43.2	1.9	0.04	—	11.38 ± 0.07	Y	$7''.7(7.7)$	1.59 ± 0.04	4.60 ± 0.08	3.01 ± 0.07
8	8.5	$22.8^{+0.3}_{-1.2}$	44.2	R	0.22	15.26 ± 0.05	13.90 ± 0.07	Y	$3''.6(3.6)$	2.18 ± 0.04	5.53 ± 0.08	3.35 ± 0.07
9	2.4	$23.1^{+0.4}_{-0.4}$	43.6	1.9	0.18	16.51 ± 0.05	15.14 ± 0.07	Y	$2''.8(3.1)$	2.35 ± 0.28	5.76 ± 0.26	3.41 ± 0.26
10	0.9	< 22.1	43.9	R	0.39	16.48 ± 0.05	14.97 ± 0.07	Y	$2''.9(2.9)$	2.66 ± 0.28	5.83 ± 0.26	3.17 ± 0.26

^a 5-10 keV flux in units of 10^{-13} erg cm $^{-2}$ s $^{-1}$; ^b log of intrinsic absorbing column density in units of cm $^{-2}$, assuming an intrinsic photon index $\Gamma = 1.8$ (see paper I) and the absorber at the redshift of the source; ^c log of the intrinsic (deabsorbed) 5-10 keV luminosity in units of erg s $^{-1}$, assuming $H_0=50$ and $q_0=0$ (see paper I); ^d optical spectral type: 1.9 – narrow line spectrum with broad component of H α , L – LINER, B – broad line QSO with blue continuum, R – broad line QSO with red continuum;

^e Photometry extracted with a circular aperture down to the noise and corrected for Galactic extinction. ^f Y if resolved in the near-IR images; ^g full-width at half-maximum along the major axis in arcseconds (quantities in brackets are in seeing units); ^h in the same errorbox of #1.

at $z = 0.26$. The dashed line gives mixed QSO-galaxy contribution models in steps of 10% relative contribution (black dots) to the rest-frame V band, down to a minimum galactic contribution of 50%. We see that even the blue QSOs are redder than usual, and the sources with bent, non-powerlaw spectra are all and only those with extended images. Also, a QSO template cannot explain all our data, irrespective of the amount of reddening. Instead, the reddest objects have colors similar to those expected from an evolved stellar population.

As an additional check, we compared the observed optical to near-IR photometry and optical spectra of each single object with those expected from (reddened) QSOs and from evolved stellar populations. An example of this method for a specific object is given in Vignali et al. (2000). The combination of the (reddened) AGN and of the galactic component should give an acceptable fit of the observed photometric points. We also request that the model matches the shape of the observed optical spectrum (paper III) with a maximum tolerance of about 30% (to allow for uncertainties introduced by the non-parallactic angle of the slit). Finally we also tried to fit the equivalent width of the observed broad hydrogen lines, or to meet their upper limits, within a factor of two (given the EW spread observed in optical samples of QSOs). QSO and stellar population templates are the same as for Fig. 1 (notes 1 and 2). The free parameters of the model are the reddening of the QSO, the age of the stellar population and the relative contribution of these two components.

Fig. 2 shows examples of our spectral fits. They refer to three representative sources, i.e. the bluest QSO (#1), a “transition” source (#6), located around the bend in Fig. 1, and the reddest object of our sample (#10). The thin solid line in the upper panels is the best fit QSO+galaxy model, the two thick lines indicate the shape

(and spread) of the line-free continuum observed in the optical spectra, while points with errorbars are the photometric fluxes normalized to R. One sees clearly the 4000 Å break in the red, spatially resolved sources, with a dis-

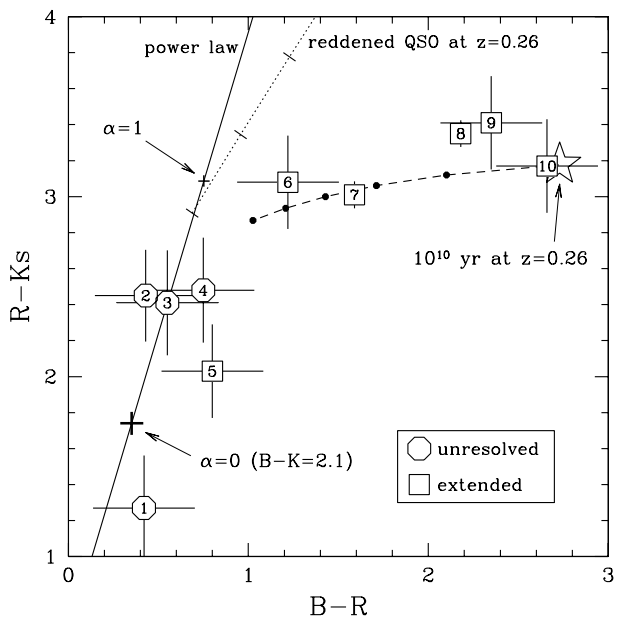


Fig. 1. R-Ks vs B-R color for the sources in our sample (see text). The numbers refer to the identifications given in Tab. 1. The dotted line gives the reddening curve of a QSO at $z=0.26$ and starts from $A_V=0.5$; marks are at $A_V=0.5, 1.0$ and 1.5 . The dashed line gives the expected colors for a model including the contribution of a QSO and an old stellar population (both at $z=0.26$); black dots give a galactic contribution (to the rest frame V-band) of 50%, 60%, 70%, 80% and 90% (the star gives the colors of the stellar template with no AGN contribution).

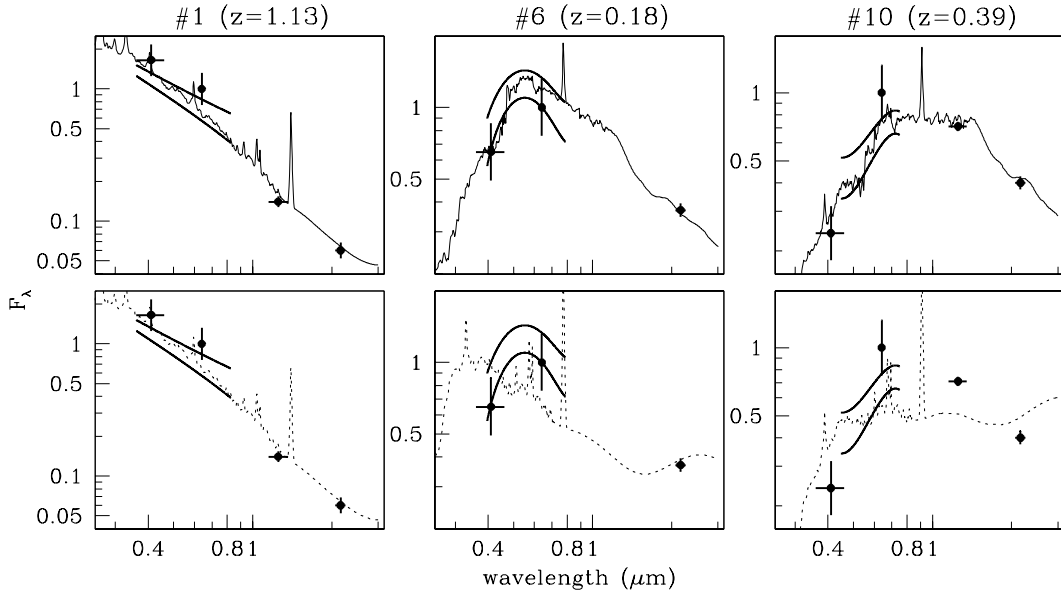


Fig. 2. Comparison between photometric measurements (black dots with errorbars) and observed optical spectral shapes (thick lines) with the best fit models for three representative objects (see text). Models in the upper panels (thin solid lines) include both the contribution from a reddened QSO and from an evolved stellar population; the latter is dominant in #6 (10^9 yr) and in #10 (10^{10} yr). Lower panels (dotted lines) are the best fit using only a QSO template with the appropriate reddening.

cernible progression from the “transition” sources to the very red ones. Along the progression, the B–R color increases from ~ 1 to ~ 2.8 and the preferred age for the model population increases from 10^9 to 10^{10} years. The fractional contribution of the reddened AGN (to the rest frame V-band) decreases from 100% in the bluest objects to a few percent in the red ones. Although the small contribution from a reddened AGN is required even in the reddest objects, this cannot dominate their red colors. This is clearly shown by the dotted lines in the lower panels of Fig. 2, which give the best fit to the photometric points using only a (reddened) QSO template: either the continuum shape or the photometric points, or both, are poorly fitted. The best model fitting to the photometry and spectral shape is in perfect agreement with the imaging results, in the sense that the contribution of the host galaxy is dominant in those sources which appear extended. Finally, it is interesting to note that the best fitting stellar populations are generally old/evolved. However, one should bear in mind that in certain cases different models such as a reddened 10^9 year old population or a reddened continuous burst provide also an acceptable fit to the data, indicating some degree of degeneracy.

Red, absorbed AGNs are about half of the identified sources in the HELLAS sample, which in turn are about two thirds of the examined errorboxes. The fraction of these obscured AGNs is expected to increase significantly at fainter X-ray fluxes, where the remaining 70–80% of the hard X-ray background is produced (eg. Gilli et al. 1999). As a consequence, our result suggests that a large frac-

tion of the hard XRB contributors have optical/near-IR counterparts which appear as “normal” galaxies (possibly with narrow AGN-like emission lines). A population of red AGNs similar to that analyzed in this paper but at $z>1$ would probably remain undetected at $R=20$. These might be the counterparts of the HELLAS sources for which no optical identification was found.

Ours are among the first red QSOs selected in hard X-rays, while previous samples have been selected in the radio (e.g. Webster et al. 1995) or in the soft X-rays (Kim & Elvis 1999). The prevalent interpretation in the latter cases is that the continuum of the red QSOs comes from the QSOs themselves, seen through an appropriate amount of reddening material (eg. Masci et al. 1998, Kim & Elvis 1999). In the case of our objects most of the continuum is instead due to the host galaxy, and absorption is needed only to make the galaxy’s the dominant contribution. Both Figs. 1 and 2 show that the reddened QSOs interpretation is untenable, since reddened QSO models fail to fit colors and spectral shapes. Also, all of them have extended IR images. The discrepancy with Masci et al. (1998) and Kim & Elvis’ (1999) results is probably to ascribe to the tendency of their selection criteria to find QSO that are on average less absorbed than ours (hence the QSO, although reddened, still dominates over the galaxy): Kim & Elvis select their red QSOs among bright soft X-ray sources, while Masci et al. select flat-spectrum radio sources that, according to the unified model, should be preferentially seen pole-on. Other studies, which use selection criteria less sensitive to absorp-

tion, as in our case, find red QSOs whose continuum is dominated by their host galaxies, in agreement with what found by us. Among these studies, Benn et al. (1998) find host galaxy-dominated red QSOs in radio sources which have steep radio spectra (hence preferentially edge-on according to the unified model). Hasinger et al. (1999) and Lehmann et al. (2000) find several red-AGNs among faint ROSAT sources whose red colors are ascribed to the contribution from their hosts; in some of these sources the redshift moves the rest frame hard-X band into the soft band, while in low-z objects the depth of the X-ray observation could detect the soft excess of obscured systems. Finally, Kruper & Canizares (1989) also found a large fraction of red-AGNs that are probably dominated by their host galaxies by selecting sources at X-ray energies (0.5–4.5 keV) higher than ROSAT. Our finding on red QSOs is in line with the results of Benn et al. (1998), Lehmann et al. (2000) and Kruper & Canizares (1989),

4. Conclusions

We presented new near-IR (J and Ks band) observations of a sample of 10 objects selected in the hard X-rays (5–10 keV). These sources were discovered in a large survey (HELLAS) performed by the BeppoSAX satellite, which resolves $\sim 20 - 30\%$ of the hard X-ray background. The sample includes 4 blue broad line QSOs and 6 AGNs with redder continua whose optical emission line spectra range from broad line objects (red QSOs), to intermediate type 1.9 AGNs, to LINER.

The B–K color ranges from the standard value of ~ 2 (typical of U–B color selected QSOs) up to ~ 6 , similar to the color of red QSOs found in radio surveys.

The red AGNs show extended near-IR images. Model fitting of the photometry and spectral data shows that all and only the red AGNs are *dominated by the emission of the host galaxy* (with an age of 10^9 – 10^{10} yr). Red AGNs amount to about a third of the total HELLAS sources, and their fraction is expected to increase significantly at fainter X-ray fluxes, where most of the hard X-ray background is produced. Therefore, our result suggests that a significant fraction of the counterparts of the sources making the hard X-ray background appear as “normal” galaxies at optical and near-IR wavelengths. Chandra and XMM are expected to discover a large number of this class of objects.

Acknowledgements. We thank the TNG staff and C. Baffa for technical assistance during the observations. We are grateful to P. Giommi, G. Matt, S. Molendi and G.C. Perola, who are involved in the HELLAS project. This work was partially supported by the Italian Space Agency (ASI) through the grant ARS-99-75 and by the Italian Ministry for University and Research (MURST) through the grant Cofin-98-02-32.

References

Benn C.R., Vigotti M., Carballo R., Gonzalez-Serrano J.I., Sánchez S.F., 1998, MNRAS 295, 451
 Bruzual A.G., Charlot S., 1993, ApJ 405, 538
 Comastri A., Setti G., Zamorani G., Hasinger G., 1995, A&A 296, 1
 Comastri A., Fiore F., Giommi P., et al., 2000, Adv. Sp. Res. 25, 833
 Elvis M., Wilkes B.J., McDowell J.C., et al., 1994, ApJS 95, 1
 Fiore, F., La Franca F., Giommi P., et al. 1999, MNRAS 306, L55 (paper I)
 Fiore F., Giommi P., Vignali C., et al., 2000, MNRAS submitted (paper II)
 Francis P.J., Hewett P.C., Folts C.B., et al., 1991, ApJ 373, 465
 Gilli R., Risaliti G., Salvati M., 1999, A&A 347, 424
 Hasinger G., Lehmann I., Giacconi R., Schmidt M., Trumper J., Zamorani G., 1999, In: Aschenbach B., Freyberg M.J. (eds.) Highlights in X-ray Astronomy. MPE Report 272, p. 199
 Hunt L., Testi L., Borelli S., Maiolino R., Moriondo G., 1994, Arcetri Technical Report, N. 4/1994
 Kim D.-W., Elvis M., 1999, ApJ 516, 9
 Kruper J.S., Canizares C. R., 1989, ApJ 343, 66
 La Franca F., Fiore F., Giommi P., et al., 2000, in prep. (paper III)
 Lehmann I., Hasinger G., Schmidt M., et al., 2000, A&A 354, 35
 Lisi F., Baffa C., Biliotti V., et al., 1996, PASP 108, 364
 Masci F.J., Webster R., Francis P.J., 1998, MNRAS 301, 975
 Matthews K., Soifer B.T., 1994, In: I. McLean (ed.) Infrared Astronomy with Arrays. Kluwer, Dordrecht , p.239
 Pompilio F., La Franca F., Matt G., 2000, A&A 353, 440
 Rowan-Robinson M., 1999, In: The Universe as seen by ISO, ESA Sp. Pub. Ser. (SP-427), in press
 Vignali C., Mignoli M., Comastri A., Maiolino R., Fiore F., 2000, MNRAS in press (astro-ph/0002279)
 Webster R.L., Francis P.J., Peterson B.A., Drinkwater M.J., Masci F.J. 1995, Nat 375, 469